Density functional theory calculations of H_2O adsorption monolayer on a Pt(111) surface

Jun HARUYAMA and Osamu SUGINO

The Institute for Solid State Physics, The University of Tokyo, Kashiwa-no-ha, Kashiwa, Chiba 277-8581

Toshiki SUGIMOTO

Department of Materials Molecular Science, Institute for Molecular Science, Myodaiji, Okazaki, Aichi, 444-8585, Japan

Precursory Research for Embryonic Science and Technology, Japan Science and Technology Agency, Saitama 332-0012, Japan

Abstract

From a theoretical point of view, the estimation of intermediate state free energy is essential for finding more efficient electrocatalyst. To investigate the accuracy of density functional theory functionals at the metal/water interface, we focus on an ideal metal/ice system: the H_2O adsorption monolayer on a Pt(111) surface. Three DFT functionals (PBE, vdW-DF, and vdW-DF2-B86R) are used to compare the adsorption energies of √39×√39 (and √37×√37) 5·7-member ring structure with the experimental activation energy of desorption. It is found that the vdW-DF2-B86R functional slightly overestimates the Pt–H_2O interaction while others seriously underestimate it.

Furthermore, we develop a first-principles methodology for analyzing the second-order nonlinear susceptibility $\chi^{(2)}_{zzz}$ applicable for metal/adsorption systems. The calculated Im $\chi^{(2)}_{zzz}$ spectra show negative double peaks in the high-frequency region, consistent with those obtained from the measured sum-frequency generation spectra. This study provides a fundamental basis for analyzing the structure of H_2O adsorbed on metal surfaces.

1 Introduction

In electrochemistry, a metal/water interface has general importance and continued interest because of the applicability of fuel cells, water electrolysis, and so on. The conversion efficiency of an electrochemical reaction depends on the free energy landscape of its rate determining step, e.g., the oxygen reduction reaction (ORR). Therefore, to estimate the free

energy of reaction intermediate states, accurate description of the interactions between H2O molecules and a metal surface is beneficial. In this study, we focus on an experimentally well-confirmed system, i.e., H_2O adsorption monolayer on a Pt(111) surface. [1, 2] In order to investigate how accurate the interaction description of density functional theory (DFT) calculations, we compare the properties obtained by first-principles calculations and previous experiments.

At low temperatures (≈ 100 K), the growth of layered structure of adsorbed H_2O molecules (in other words, crystalline ice film) was observed on a Pt(111) surface, [3] and structural analysis methods in surface science have been applied to investigate the Pt(111)/H_2O structure. In 1997, Glebov et al. observed He-atom scattering (HAS) diffraction patterns of the H_2O adsorbed molecules on Pt(111) surface and found a well-ordered 2D ice layer with a $(\sqrt{37}\times\sqrt{37})R25.3°$ or $(\sqrt{39}\times\sqrt{39})R16.1°$ symmetry. [4] They suggested possible lateral H_2O arrangements, in which the hydrogen bonds construct 6-member rings. As well as the HAS measurement, Haq et al. obtained an equivalent low-energy electron diffraction (LEED) pattern on the first layer of H_2O adsorption molecules on Pt(111). [5] In the same study, Haq et al. showed the activation energy of desorption, $E_a = 52 \pm 2$ kJ/mol, for the adsorption layers by temperature programmed desorption (TPD) analysis. [5] Daschbach measured the desorption rates of the H_2O layers on Pt(111) by HAS and estimated the activation energy $E_a = 54.2 \pm 3$ kJ/mol, by the Arrhenius equation. [6]

In 2010, Nie et al. obtained scanning tunneling microscope (STM) images on the H_2O first layer. Inferred from an observed triangular depression, the authors proposed the first layer structure as a hexagon of H_2O molecules surrounding 5- and 7-member rings. [7, 8] From the consistency between the experimental observation and DFT calculations, we consider the structure suggested by Nie to be thermodynamically stable at low temperatures. Thus, the detailed structure and activation energy of desorption can be compared with first-principles calculations in the Pt/water system.

In this study, we confirmed the stable structure for H_2O adsorption monolayer on Pt(111) by comparing the DFT calculated adsorption energies of several model structures. The zero-point vibration energies of stable structures were considered. We further discuss the prediction accuracy of the DFT calculation for this Pt/water system.

2 Ice Ih and H_2O monolayer models

For the discussion of functional accuracies, we evaluated the lattice energy E_{lat} in bulk ice (Ih phase), which is defined using the DFT total energy E_{DFT}:

$$E_{lat} = -\{E_{DFT}(n\mathrm{H_2O}) - nE_{DFT}(\mathrm{H_2O})\}/n \quad (1),$$

where $n\mathrm{H_2O}$ and $\mathrm{H_2O}$ represent the systems of ice Ih and an isolated H_2O molecule,

respectively. Here, the Bernal–Fowler periodic model was employed as the structure of Ih phase. [9] The resulted values by using three DFT functionals, PBE, [10] vdW-DF, [11] and vdW-DF2-B86R, [12] are listed in Table 1.

Table 1. Lattice parameter ratios c/a, cell volumes V (Å^3/H_2O), and lattice energies E_{lat} (meV/H_2O). Experimental values are taken from refs. [13, 14].

Functional	c/a	V_0	E_{lat}
PBE	1.634	29.90	655
vdW-DF	1.635	33.19	582
vdW-DF2-B86R	1.632	29.41	697
Experiment	1.629	32.55	580

The lattice parameters and energies of PBE and vdW-DF are consistent with those of previous DFT studies. [15, 16] The lattice energy of vdW-DF is good agreement with the experimental value, and those of PBE and vdW-DF2-B86R are overestimated it c.a. 100 meV/H_2O. It is worth noting that these estimated accuracies of the H_2O–H_2O interaction cannot be invoked for the Pt–H_2O interaction.

In addition to the H_2O–H_2O interaction, it is also ambiguous whether the metal–H_2O interaction can be correctly described by DFT calculations. Here, considering the adsorption of H_2O monolayer on Pt(111), the difference in Pt–H_2O interactions obtained by the selected functionals is discussed. The adsorption energy E_{ad} is defined as

$$E_{ad} = -\{E_{DFT}(\mathrm{Pt}/n\mathrm{H_2O}) - E_{DFT}(\mathrm{Pt}) - nE_{DFT}(\mathrm{H_2O})\}/n \quad (2),$$

where Pt/$n$$H_2O$ and Pt represent the systems of $n$$H_2O$ adsorption on the Pt(111) and pristine Pt(111) surface, respectively. We conducted DFT calculations and evaluated E_{ad} of several model monolayer structures, i.e., simple H-down configurations with $(\sqrt{3}\times\sqrt{3})R30°$ symmetry (called √3 H-up/down), realistic 6- and 5·7-ring configurations with $(\sqrt{39}\times\sqrt{39})R16.1°$ symmetry (called √39 6-ring and √39 5·7-ring) as shown in Figs. 1 (a), (b), and (c), respectively. We further considered the adsorption model with 5·7-ring with $(\sqrt{37}\times\sqrt{37})R25.3°$ symmetry. We evaluated the zero-point vibrational correction ΔE_{ZPE} and the heat of adsorption H_{ad} defined as

$$\Delta E_{ZPE} = -\{E_{ZPE}(\mathrm{Pt}/n\mathrm{H_2O}) - E_{ZPE}(\mathrm{Pt}) - nE_{ZPE}(\mathrm{H_2O})\}/n \quad (3),$$

$$H_{ad} = E_{ad} + \Delta E_{ZPE} \quad (4).$$

The zero-point vibrational energy E_{ZPE} within the harmonic approximation is evaluated by the summation of the vibrational (phonon) eigen-frequencies.

2.1 Computational details for H_{ad}

A four-layer slab of Pt(111) was constructed by cutting face-centered cubic (fcc) crystals. We fixed the lattice constant of the Pt(111) surface at an experimental value of 3.924 Å. The Pt atom positions in the first and second bottom layers were fixed in the crystal positions. The VESTA

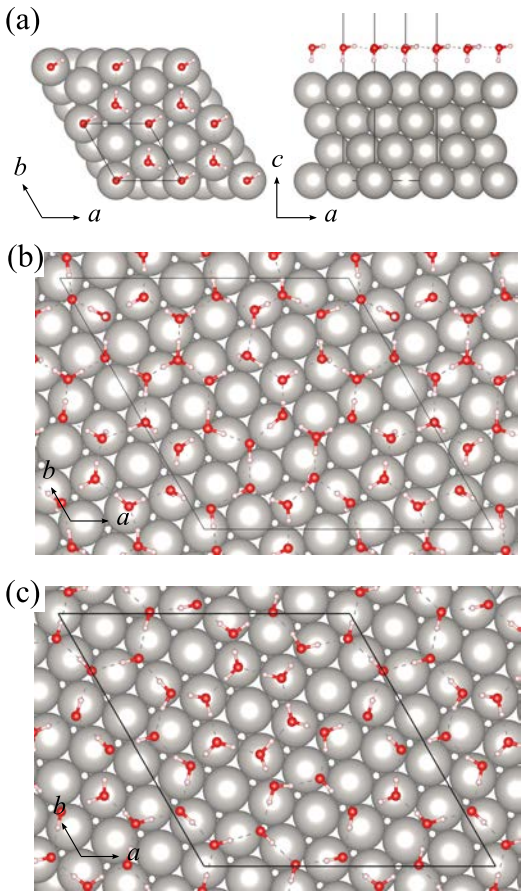

Fig 1. Structures of H_2O monolayer: (a) √3 H-down, (b) √39 6-ring, and (c) √39 5·7-ring. Adapted with permission from ref. [17]. Copyright 2024 American Physical Society.

package was used for visualization of atom coordinates. [18] Quantum ESPRESSO (QE) code [19] was used to perform spin-unpolarized DFT calculations. The cutoff energies were set to 40 and 320 Ry for the wave functions and the augmented charge, respectively. In surface slab calculations, converged k-point samplings of 12×12×1, 4×4×1, and 4×4×1 were adopted for the √3, √39, and √37 cells, respectively. Vibrational frequencies and modes were obtained from the diagonalization of dynamical matrix implemented in QE. Non-shifted k-point (q-point) samplings for electronic states of 8×8×1 (4×4×1), 1×1×1 (1×1×1), and 1×1×1 (1×1×1) were adopted for √3, √39, and √37 cells, respectively. The raw data of the structures obtained are made available in the ISSP data repository. [20]

3 Results of adsorption energies

Table 2 shows the obtained adsorption energies E_{ad} in this study. E_{ad} of the √39 6-ring was larger than that of √3 H-down by 10–25 meV/H_2O in the PBE and vdW-DF2-B86R functionals. The opposite result was obtained using vdW-DF functional. The √39 5·7-ring structure had highly ordered H_2O configurations, with perfect hydrogen bonds along surface parallel direction. In addition, 6 H_2O molecules in the √39 cell were close to the surface ($d_{Pt–O}$ = 2.21–2.25 Å), while the other H_2O molecules were located away by one step ($d_{Pt–O}$ = 3.3–4.0 Å). The latter molecules tend to point a H atom toward the surface. These features and adsorption energies indicate that the 5·7-ring structure has the largest advantage from the Pt-H_2O interaction.

Table 2 also lists the heats of adsorption H_{ad} of the √39 5·7-ring and √37 5·7-ring structures. The zero-point vibration corrections ΔE_{ZPE} of the two structures were c.a. −100 meV/H_2O. Considering a typical physisorption process of H_2O adsorption, the activation energy of the desorption can be approximated by H_{ad}.

Compared with the experiment, H_{ad} obtained by the PBE, and vdW-DF functionals underestimated the experimental value (c.a. 110–160 meV), while that obtained by vdW-DF2-B86R slightly overestimated (c.a. 40 meV). In addition, the wetting condition was satisfied by vdW-DF2-B86R only; this functional is optimal among the three functional. However, going back to the estimated errors of E_{lat} in ice Ih (see Table 1), this agreement come from the accidental cancellation about overestimation of interaction between H_2O–H_2O and underestimation between Pt–H_2O. Therefore, more accurate functional will be required to satisfy the thermodynamic condition of multilayer H_2O on Pt(111).

Table 2. Adsorption energies E_{ad}, and the heats of adsorption H_{ad}. Adapted from ref. [17].

Functional	PBE	vdW-DF	vdW-DF2-B86R
Structure	E_{ad} [meV/H_2O]		
√3 H-down	486	502	640
√39 6-ring	511	476	654
√39 5·7-ring	556	529	710
√37 5·7-ring	558	537	709
	H_{ad} [meV/H_2O]		
√39 5·7-ring	447	403	589
√37 5·7-ring	446	404	605

4 Second-order non-linear susceptibility

Recently, sum frequency generation (SFG) vibrational spectroscopy has become a frequently used method to determine the configuration of adsorbed H_2O on various metal surfaces. The heterodyne-detected SFG spectroscopy can be applied to the ice film on Pt(111) to obtain the imaginary part of the second-order nonlinear susceptibility, Im $\chi^{(2)}$, revealing the structure. [21, 22] In this study, we develop a DFT-based method for calculating $\chi^{(2)}$.

We use the sum-over-states representation of $\chi^{(2)}$ derived from perturbation theory: [23, 24]

$$\chi^{(2)}_{\alpha\beta\gamma}(\omega_{IR}) = \sum_{v} \frac{A_{\alpha\beta\gamma,v}}{\omega_v - \omega_{IR} - i\Gamma_v} \qquad (5),$$

where ω_{IR}, ω_v, and Γ_v represent the infrared (IR) frequency, vibrational frequency of the eigenmode v, and dephasing rate, respectively. The components of α, β, and γ are x-, y-, or z-direction. The numerator is defined as

$$A_{\alpha\beta\gamma,v} = \left(\sum_{\kappa,\gamma'} R_{\kappa,\alpha\beta\gamma'} U_v(\kappa,\gamma') \right) \times \left(\sum_{\kappa,\gamma} Z^*_{\kappa,\gamma\gamma'} U_v(\kappa,\gamma') \right) \qquad (6),$$

where $U_v(\kappa,\alpha)$, $Z^*_{\kappa,\alpha\beta}$, and $R_{\kappa,\alpha\beta\gamma}$ represent the displacements of vibrational eigenmodes, the Born effective-charge tensor, and the Raman tensor on an atom index κ, respectively. For the calculations of $Z^*_{\kappa,\alpha\beta}$ and $R_{\kappa,\alpha\beta\gamma}$, we used the representation of response tensors with respect to electric field $\mathcal{E}_\alpha$:

$$Z^*_{\kappa,\alpha\beta} = \frac{\partial F_{\kappa,\beta}}{\partial \mathcal{E}_\alpha} \qquad (7),$$

$$R_{\kappa,\alpha\beta\gamma} = \frac{\partial^2 F_{\kappa,\gamma}}{\partial \mathcal{E}_\alpha \partial \mathcal{E}_\beta} \qquad (8),$$

where $F_{\kappa,\alpha}$ is the Hellman-Feynman force. By modifying the effective-screening medium (ESM) method to apply $\mathcal{E}_z$ along surface normal

direction, [25] eqs. (7) and (8) can be evaluated using the finite difference method.

4.1 Computational details for $\chi^{(2)}$

The ESM boundary condition of the metal/vacuum/metal system was used under a finite electric field. [25] $Z^*_{\kappa,\alpha\beta}$ and $R_{\kappa,\alpha\beta\gamma}$ were obtained using the 4- and 5-point central-finite-difference formulae, respectively. $\Delta\mathcal{E}_z$ was set to 0.005 Ry/e·bohr. The dephasing rate Γ_ν was set to 30 cm^{-1} in eq. (5).

5 Results of second-order non-linear susceptibility: H_2O monolayer on Pt(111)

Figure 2 shows $\mathrm{Im}\,\chi^{(2)}_{zzz}$ of the √39 5·7-ring structure. The PBE and vdW-DF2-B86R functionals gave qualitatively similar results. The intensity at greater than 3000 cm^{-1} region was significantly higher than that at lower region. The large negative amplitude of $\mathrm{Im}\,\chi^{(2)}_{zzz}$ at this region can be attributed to the stretching modes of the H-down molecules. This trend is consistent with those of water and ice surfaces. [21–24]

We compared the calculated spectra of $\mathrm{Im}\,\chi^{(2)}_{zzz}$ with the √39 5·7-ring structure by vdW-DF2-B86R functional with the heterodyne-detected SFG spectroscopy. [21, 22] The first-highest amplitude peak located around 3430 cm^{-1} is in good agreement with the SFG peak positions of 0.8 and 1.4 BL samples (~ 3370 cm^{-1}). The second-highest peak at 3250 cm^{-1} is also in reasonable agreement with the peak positions of 0.8 and 1.4 BL samples (3290–3300 cm^{-1}). The results suggest that the experimental peak at

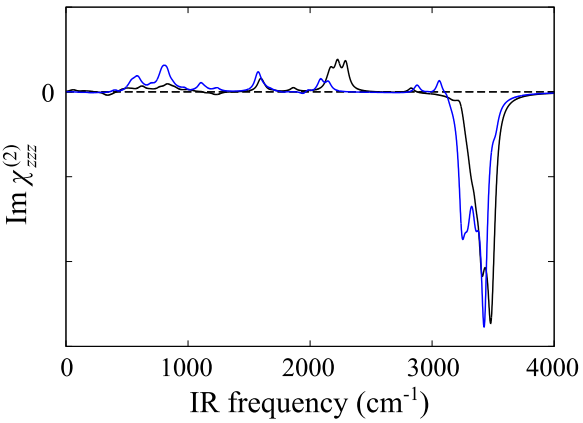

Fig 2. $\mathrm{Im}\,\chi^{(2)}_{zzz}$ as a function of IR frequency ω_{IR}. The amplitudes obtained by PBE and vdW-DF2-B86R functionals are shown as black and blue lines, respectively. Adapted with permission from ref. [17]. Copyright 2024 American Physical Society.

3280 cm^{-1} of 2.6 BL could be come from the OH stretching mode of bulky surface layers. To determine which vibrational mode contributes to the negative amplitude, the vibrational density of states of √39 5·7-ring structures were projected onto center 6-ring, upper 5-ring, and the other 6·7-ring H_2O molecules. The DOSs of the two structures at 3250 cm^{-1} are exclusively composed of the 5-ring and 6·7-ring H_2O molecules. Such analysis is useful to attribute $\chi^{(2)}$ spectral to characteristic modes and atoms.

To the best of our knowledge, $\mathrm{Im}\,\chi^{(2)}_{zzz}$ of Pt(111)/ice system at low-frequency region (ω_{IR} < 3000 cm^{-1}) has not been observed by SFG measurements; however, the first-principles

method developed in this study can provide all frequency region. The small positive amplitude of Im $\chi^{(2)}_{zzz}$ in the low-frequency region was predicted as shown in Fig. 2. For the stretching modes at ω_{IR} = 1800–2400 cm^{-1}, the connected 5-ring H_2O molecules include H-up H_2O molecules, which results in a positive amplitude. For the bending and libration modes at 1600 and 600–1200 cm^{-1}, respectively, a qualitative one-molecule description can be used to explain the sign of Im $\chi^{(2)}_{zzz}$, as follows; we consider the bending and libration (rotation around *y*-axis) motions of one H-down H_2O molecule as shown in Fig. 3. For the bending motion, the *z*-component amplitude of H1 atom is negligible. On the other hand, the *z*-component amplitude of H2 atom is finite. Because the OH direction of the contributed H atom are upward, the positive sign of Im $\chi^{(2)}_{zzz}$ is expected. In the same way, for the libration motion, the downward H1 and upward H2 atoms have no and positive contributions to Im $\chi^{(2)}_{zzz}$, respectively.

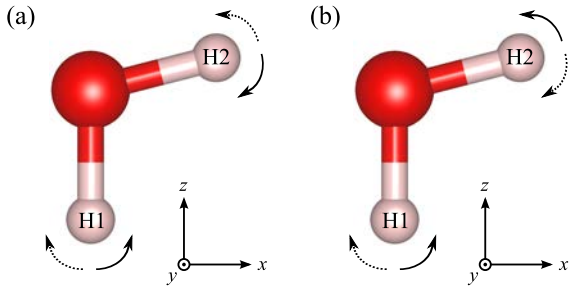

Fig 3. Schematic images of (a) bending and (b) libration motions of one H-down H_2O molecule. Reprinted with permission from ref. [17]. Copyright 2024 American Physical Society.

6 Conclusions

The adsorbed H_2O monolayers on Pt(111) surface were treated within first-principles methods. The adsorption energies E_{ad} of √3 H-down, √39 6-ring, √39 (and √37) 5·7-ring structures were calculated by three (PBE, vdW-DF, and vdW-DF2-B86R) functionals. It is indicated that the 5·7-ring structure has great advantage of the interaction energies between Pt–H_2O and H_2O–H_2O. The heats of adsorption H_{ad} of √3 H-down, √39 5·7-ring, and √37 5·7-ring structures show that the vdW-DF2-B86R functional is the most reliable one among them. In addition, the second-order nonlinear susceptibility $\chi^{(2)}_{zzz}$ was obtained by developing the ESM + applied field approach. The negative and positive amplitudes of Im $\chi^{(2)}_{zzz}$ were obtained in the high and low frequency regions, respectively. The spectra calculated with the √39 5·7-ring structure were consistent with SFG spectroscopy. This study paved the way for the understanding of metal-adsorbed water and electrochemical interfacial systems.

References

[1] J. Carrasco, A. Hodgson, and A. Michaelides, Nat. Mater. **11**, 667 (2012).

[2] A. Groβ and S. Sakong, Chem. Rev. **122**, 10746 (2022).

[3] N. Materer, U. Starke, A. Barbieri, M A. Van Hove, G. A. Somorjai, G.-J. Kroes, and C. Minot, J. Chem. Phys. **99**, 6267 (1995).

[4] A. Glebov, A. P. Graham, A. Menzel, and J.

P. Toennies, J. Chem. Phys. **106**, 9382 (1997).
[5] S. Haq, J. Harnett, and A. Hodgson, Surf. Sci. **505**, 171 (2002).
[6] J. L. Daschbach, B. M. Peden, R. S. Smith, and B. D. Kay, J. Chem. Phys. **120**, 1516, (2004).
[7] S. Nie, P. J. Feibelman, N. C. Bartelt, and K. Thümer, Phys. Rev. Lett. **105**, 026102, (2010).
[8] P. J. Feibelman, N. C. Bartelt, S. Nie, and K. Thümer, J. Chem. Phys. **133**, 154703 (2010).
[9] D. R. Hamann, Phys. Rev. B **55**, R10157 (1997).
[10] J. P. Perdew, K. Burke, and M. Ernzerhof, Phys. Rev. Lett. **77**, 3865 (1996).
[11] M. Dion, H. Rydberg, E. Schröder, D. C. Langreth, and B. I. Lundqvist, Phys. Rev. Lett. **92**, 246401 (2004).
[12] I. Hamada, Phys. Rev. B **89**, 121103(R) (2014).
[13] V. R. Brill and A. Tippe, Acta Cryst. **23**, 343 (1967).
[14] E. Whalley, Trans. Faraday Soc. **53**, 1578 (1957).
[15] P. J. Feibelman, Phys. Chem. Chem. Phys. **10**, 4688 (2008).
[16] I. Hamada, J. Chem. Phys. **133**, 214503 (2010).
[17] J. Haruyama, T. Sugimoto, and O. Sugino, Phys. Rev. Materials **7**, 115803 (2023).
[18] K. Momma and F. Izumi, J. Appl. Crystallogr. **44**, 1272 (2011).
[19] P. Giannozzi *et al*., J. Phys.: Condens. Matter **21**, 395502 (2009); *ibid.* **29**, 465901 (2017).
[20] https://isspns-gitlab.issp.u-tokyo.ac.jp/j-haruyama/Pt111_H2O-monolayer
[21] T. Sugimoto, N. Aiga, Y. Otsuki, K. Watanabe, and Y. Matsumoto, Nature Phys. **12**, 1063 (2016).
[22] T. Sugimoto and Y. Matsumoto, Phys. Chem. Chem. Phys. **22**, 16453 (2020).
[23] A. Morita and J. T. Hynes, Chem. Phys. **258**, 371, (2000).
[24] A. Morita and J. T. Hynes, J. Phys. Chem. B **106**, 673, (2002).
[25] M. Otani and O. Sugino, Phys. Rev. B **73**, 115407 (2006).